The sensitive surface chemistry of Co-free, Ni-rich layered oxides: identifying experimental conditions that influence characterization results

The sensitive surface chemistry of Co-free, Ni-rich layered oxides: identifying experimental conditions that influence characterization results

Linqin Mu[a*], Zhenzhong Yang[b], Lei Tao[a], Crystal K. Waters[a], Zhengrui Xu[a], Luxi Li[c], Sami Sainio[d], Yingge Du[b], Huolin L. Xin[e], Dennis Nordlund[d], and Feng Lin[a*]

a) Department of Chemistry, Virginia Tech, Blacksburg, VA 24061, USA

b) Physical and Computational Sciences Directorate, Pacific Northwest National Laboratory, Richland, WA 99352, USA

c) Advanced Photon Source, Argonne National Laboratory, Argonne, IL 60439, USA

d) Stanford Synchrotron Radiation Lightsource, SLAC National Accelerator Laboratory, Menlo Park, CA 94025, USA

e) Department of Physics and Astronomy, University of California, Irvine, CA 92697, USA

*Corresponding Authors
Email: linqinmu@vt.edu
Email: fenglin@vt.edu

Abstract

Recent studies have suggested that Co-free, Ni-rich layered cathodes (e.g., doped $LiNiO_2$) can provide promising battery performance for practical applications. However, these layered cathodes suffer from significant surface instability during various stages of the sample history, which generates inherent challenges for achieving stable battery performance and obtaining statistically representative characterization results. To reliably report the surface chemistry of these materials, delicate controls of stepwise sample preparation are required. In this study, we aim to illustrate how the surface chemistry of $LiNiO_2$ based materials changes with various environments, including human exhalation, sample storage, sample preparation, electrochemical cycling, and surface doping. Our results demonstrate that the surface of these materials is highly reactive and prone to alter at various stages of sample handling and characterizations. The sensitive surface could impact the interpretation of the surface chemical and structural information, including surface carbonate formation, transition metal reduction and dissolution, and surface reconstruction. Importantly, the heterogeneity of the surface degradation calls for a consolidation of nanoscale, high-resolution characterization and ensemble-averaged methods in order to improve statistical representation. Furthermore, the doping chemistry can effectively mitigate the surface degradation and improve overall battery performance due to the enhanced surface oxygen retention. Our study highlights the necessity of strict measurements through complementary characterizations at multiple length scales to eliminate unintentional biased conclusions.

Keywords: surface chemistry, Co-free Ni-rich cathodes, instability, sample handling and preparation

Introduction

High energy density lithium ion batteries have been applied as the main energy storage technology in portable devices and green transportations. $LiCoO_2$, a layered oxide cathode in lithium ion batteries, has obtained unprecedented success since its commercialization in the 1990s. $LiNiO_2$, isostructural to $LiCoO_2$, can deliver a higher capacity within a relatively low upper cutoff voltage.[1] However, its practical application has been hindered due to the inherent structural instability.[1-3] Thus, cobalt, as an essential element, has been incorporated into the $LiNiO_2$ system to form $LiNi_{1-x-y}Mn_yCo_xO_2$ (NMC) and $LiNi_{1-x-y}Co_xAl_yO_2$ (NCA) materials to release the strong magnetic moment and ultimately stabilize the structure.[4, 5] At present, researchers are pursuing the theoretical capacity of NMCs either by elevating the high cutoff voltage or increasing the nickel concentration. However, these strategies have inevitably provoked some of the degradation pathways of these materials, including transition metal reduction/dissolution, surface reconstruction, gas evolution, electrolyte oxidation/decomposition, and chemomechanical breakdown.[6-10] Additionally, most of these materials are synthesized in the polycrystalline form and have heterogeneous chemistry, resulting in high heterogeneous degradation patterns.[7, 11]

Aiming to achieve higher energy batteries, researchers have started to revisit the $LiNiO_2$ chemistry with hopes that knowledge obtained from NMC and NCA studies could be applied to $LiNiO_2$ and resolve the issues that were identified decades ago.[1] Furthermore, eliminating the use of cobalt can circumvent the issues surrounding Co such as high toxicity, high cost, and child labor abuse in mining.[4, 12] At the material level, the most popular strategy is the bulk cationic doping to enhance the electrochemical reversibility.[13-17] With doping strategies, Co-free Ni-rich layered cathode materials are expected to deliver comparable battery performance to NMCs and NCAs.[12] In addition, many studies have been performed on modulating the electrolyte composition to improve the electrode-electrolyte interphase for stabilizing the battery performance.[7, 18-20] The surface of $LiNiO_2$-based materials is much more reactive than NMC and NCA materials owing to the extreme Ni^{3+}/Ni^{4+} redox couple. Thus, revealing the origins of surface changes can better inform the advanced design of promising $LiNiO_2$-based materials. At present, most studies rely on *ex situ* characterization methods to understand the surface degradation of cathode materials, for example, transition electron microscopy (TEM) based techniques for atomic scale structural and chemical analysis, as well as surface sensitive X-ray spectroscopy for ensemble-averaged measurements to probe surface chemical information. The surface sensitive probing techniques

typically have low penetrating depths, which makes it difficult to study surface chemistry under practical battery operating environments. Noticeably, the chemical and structural information on the particle surface may be influenced by a range of experimental conditions, including but not limited to, human exhalation, sample storage, and sample preparation during material surface analysis. This can skew observations found in characterization analysis, surface doping, and electrochemical protocol. Therefore, to characterize the surface of $LiNiO_2$ properly, one must understand how the experimental conditions influence overall surface and interfacial chemistries.

Herein, we aim to provide a systematic study on the surface challenges of Co-free, Ni-rich layered cathode materials by combining our experimental observations with other studies in the literature. The surface chemistry is investigated and compared using a suite of synchrotron/electron spectroscopic and imaging techniques under various sample conditions. We report that the sample preparations greatly affect experimental observations due to the highly reactive cathode surface. We highlight that strict protocals are required to understand the relationship between cathode surface chemistry and battery performance, which can be potentially facilitated by carefully designed, surface-sensitive measurements. Finally, this study demonstrates that the surface doping approach can stabilize the surface chemistry and improve battery performance.

Results and Discussion

For more than a decade, researchers have known that layered oxide cathodes, particularly NMC and NCA materials, have fragile surfaces.[21] Thus, it allows various chemical/electrochemical reactions with gases (e.g., storing environments) or liquids (e.g., organic electrolytes) at the surfaces. As the urgent demand for commercialization of the Co-free, Ni-rich layered cathodes, the shelf life of active powders is considered as an important characteristic due to the uncertain delay from powder production to electrode processing and to battery manufacturing. In addition, with the nickel concentration approaching 100%, and the pursuit towards Co-free materials, surface stability against the organic electrolyte is vital in the commercialization. $LiNiO_2$-based materials are more unstable than their cobalt-containing analogs because of the increased magnetic frustration of Ni^{3+} than Co^{3+}.[4] Therefore, surface degradation is more severe in Ni-rich oxide cathodes due to the high oxidation state of nickel.[22] We previously discovered that the electrochemical performance of $LiNiO_2$ cathode can be improved by incorporating dual dopants through the surface and bulk properties enhancement.[13, 14] Herein, we

exploit the platform of LiNiO$_2$-based materials to study the surface fragility under various practical conditions. Moreover, we will further discuss advantages of doping chemistry through the post-mortem characterizations. Lastly, we are aiming to provide insights into developing low-cost, high-energy Co-free Ni-rich cathode materials.

Lithium residual species

The surface of alkali metal containing layered cathode materials are usually covered by undesired alkali metal residues (e.g., hydroxide and/or carbonate) accompanied by active oxygen species and nickel reduction.[23-26] Previous studies corroborated that sufficient lithium residuals negatively impact interfacial chemical/electrochemical reactions with conventional carbonate-based electrolytes, which is crucial to battery performance.[27, 28] To avoid introducing lithium residuals into batteries, washing or high temperature re-calcination prior to the electrode processing are the two main strategies at present.[29-31] In materials with increased concentrations of nickel, there are more lithium residuals present.[7, 32] Thus, due to the high surface sensitivity, we first studied how the atmosphere influences the surface components of LiNiO$_2$ by virtue of X-ray photoelectron spectroscopy (XPS).

Herein, we utilized three representative conditions, i.e., pristine, 30 min aging, and 30 min exhalation (**Figure S1** and **Figure 1**). The pristine represents the sample immediately transferred to the vacuum chamber for XPS measurement right after calcination (after the temperature naturally decreased to room temperature in the tube furnace with oxygen flow). The abbreviations "30 min aging" and "30 min exhalation" represent the as-synthesized LiNiO$_2$ stored for 30 minutes in ambient environmental conditions and under continuous human exhalation in ambient environment, respectively. There are three spectra (C*1s*, Li*1s*, and O*1s*) related to the lithium residuals in the survey XPS spectra. In order to simplify the comparison, here, we deconvoluted the C*1s* peak (**Figure 1a**) into two main groups: organic carbon groups and inorganic carbonates (-CO$_3$) that locate below 288 eV and above 289 eV, respectively. The organic carbon groups (COOH, C=O, C-O, and C=C) might come from adventitious carbonaceous species and carbon tape, whereas the peak centered at 289 eV can be associated with Li$_2$CO$_3$.[33] The peak area of the Li$_2$CO$_3$ has a strong contribution to ~34.48%, 39.62%, and 43.48% in the C1s spectra of the pristine, 30 min aging, and 30 min exhalation samples. The Li1s spectrum can be associated with a low binding energy component from the lattice Li in LiNiO$_2$ along with the undesired surface

residal species of LiOH and Li_2CO_3. The peaks area of Li_2CO_3 and LiOH contributes ~58.73%, 60.56%, and 95.16% in the Li1s spectra of the pristine, 30 min aging, and 30 min exhalation samples (**Figure 1b**). In addition, the peak proportion representing $LiNiO_2$ decreases dramatically in the 30 min exhalation sample (**Figure 1b**). Furthermore, a similar trend can be observed in the O1s spectra, displaying the proportion of residual species (Li_2CO_3 and LiOH) to be 66.3%, 72.3%, and 90.8%, respectively (**Figure 1c**). Concurrently, the lattice oxygen proportions were reduced from 33.7% to 27.7%, and all the way down to 9.2% for the exhalation sample.
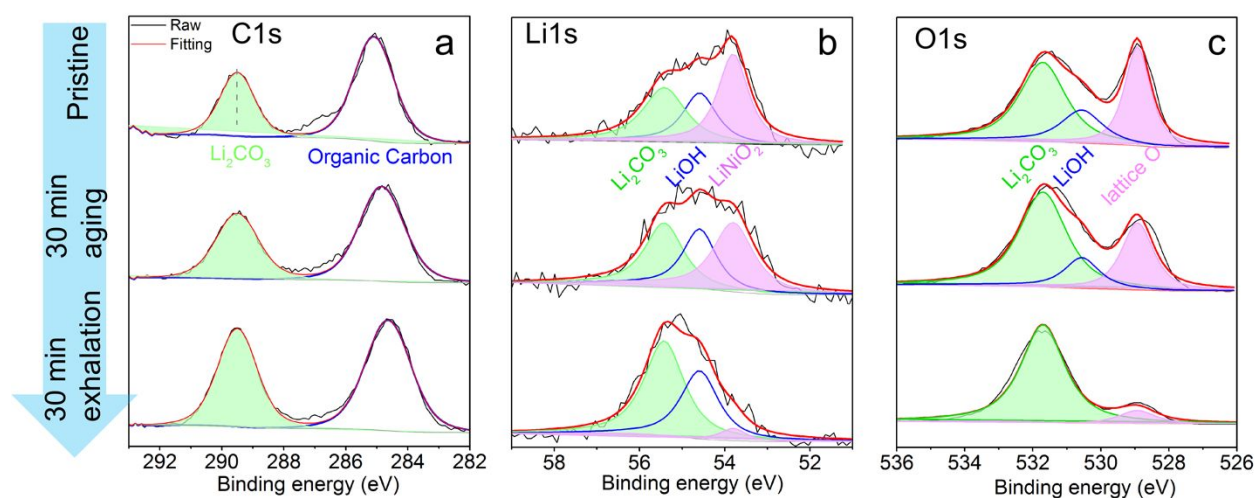
Figure 1 XPS spectra of $LiNiO_2$ samples under various conditions, i.e., pristine, 30 min aging, and 30 min exhalation; **a)** C*1s* spectra that are deconvoluted into Li_2CO_3 and organic carbon groups **b)** Li*1s* spectra that are deconvoluted into Li_2CO_3, LiOH, and $LiNiO_2$, and **c)** O*1s* spectra that are deconvoluted into Li_2CO_3, LiOH, and lattice oxygen (Li-O and Ni-O).[33]

By comparing the C*1s*, Li*1s*, and O*1s* XPS spectra and the corresponding area proportions, we found corroborative results. Firstly, a great amount of residual carbonate on the pristine $LiNiO_2$ surface illustrates the continued challenge in avoiding carbonate formation during calcination and quick transferal. There was a clear increase in inorganic carbonates (C*1s*, Li*1s*, and O*1s* XPS spectra) concurrent with the decrease of lattice Li and O proportions after exposure to ambient environment, which was amplified under continuous human exhalation (lattice Li and O are almost negligible on the surface) (**Figure 1**). This is indicative of the continuous formation of inorganic carbonates, which strongly attenuates the photoelectron signals from underneath $LiNiO_2$ layers. Our observertion is consistent with previous studies suggesting that dense concentration of water

and CO_2 on the oxide cathode surface facilitates chemical reactions to yield increased amounts of surface inorganic carbonates.[34] Previous studies have shown the surface chemical bonding and structure of NMC materials are readily transformed by certain environments, including CO_2, H_2O, O_2, and other reactive gases in a glove box.[27,35-38,] These gases react with layered oxides by extracting lithium from the lattice, further generating LiOH and/or Li_2CO_3 as well as oxygen vacancies. Lithium residuals on NMC and NCA materials also have been confirmed by infrared spectroscopy, Raman spectroscopy, and TEM.[27, 30, 34, 39] It is a consensus that surface instability is one of the common challenges for many battery materials.[40] Other materials, such as sodium-containing layered cathode materials and Li-rich materials, also encounter surface-air instability, which leads to Na/Li residual formation and elevated pH on the particle surfaces. For sodium-containing layered cathode materials, water intercalation or Na^+/H^+ exchange also takes place, which can disrupt the layered structure.[39] These changes would trigger slurry alkalization, degassing problem, and electrolyte decomposition. Based on our results and previous findings, we recommend that the details about sample handling should be specified in the journal publications, especially those involving delicate surface chemical analysis.

Long-term sample storage

Chemical reactions during storage generate electrically insulating carbonate which elevates internal cell resistance and also alters the surface morphology.[25, 38, 41] The electronic and ionic insulation of carbonate induces a sequence of chemical/electrochemical reaction behaviors.[16] For instance, the transformed Lewis base surfaces can react with electrolytic species, generating detrimental species such as HF and gases.[7, 21 24] Therefore, extra cautions are required when preparing or handling $LiNiO_2$-based materials before the battery assembly (**Figure 1**). Herein, we evaluate the battery performance of the $LiNiO_2$ cathode after storage in the dry box (humidity: ~30%) and Ar glove box (the water level was ~0.5 ppm) for two weeks. Two weeks would be a reasonable time frame between the synthesis of cathode powders and their processing into batteries in the actual manufacturing.
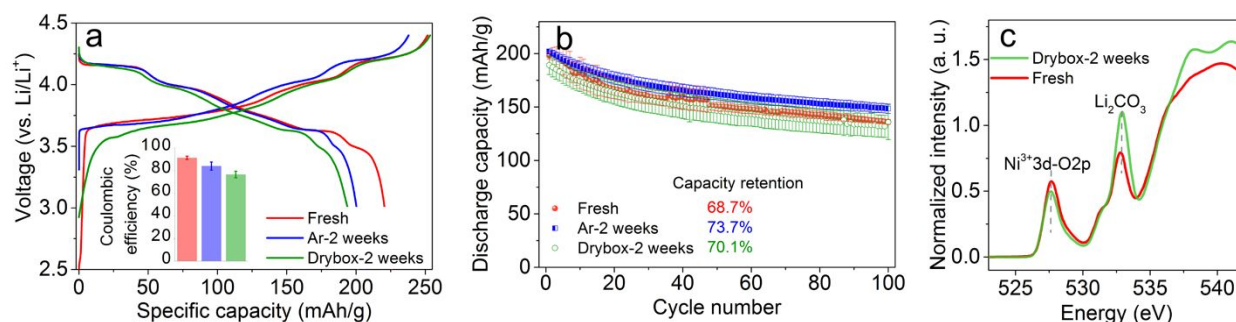
Figure 2 Cycling performance of the LiNiO$_2$ cathode after storing under various conditions, including fresh, Ar glovebox for two weeks, and dry box for two weeks. The data illustrates **a**) representative first charge/discharge profiles at C/10, insert is the histogram of the initial Coulombic efficiency (the colors are corresponding to the voltage profiles) presented with error bars, which are created based on the standard deviation of at least three repeated measurements; **b**) cycling stability within 2.5–4.4 V vs Li/Li$^+$ at C/3 at 22 °C, the performance was averaged by three individual cells. The formation cycle was at C/10 within 2.5–4.4 V vs Li/Li$^+$ at 22 °C . **c**) Soft XAS (X-ray absorption spectroscopy) O K-edge spectra in the TEY (total electron yield) mode, the distinct peak intensity located at ~534 eV of the sample stored in dry box for two weeks that can be associated with the carbonate accumulation. (Note that the lowest energy resonance of water is at 535 eV.)

The initial discharge capacity of the aged samples after Ar glovebox and dry box storage are ~200 mAh/g (**Figure 2a**), which are slightly lower than that of the fresh sample (~225 mAh/g). This is likely due to the carbonate formation that consumes reversible lithium at the particle surface. The increase of carbonate species is shown by the soft XAS (X-ray absorption spectroscopy) O K-edge (**Figure 2c**). When comparing the samples – fresh, Ar glovebox storage, and dry box storage – the initial Coulombic efficiency was approximately 91%, 85%, and 76%, respectively (**Figure 2a insert**). It is consistent with the literature that carbonate impurities readily decompose above 3.8V vs Li/Li$^+$, leading to a much lower initial Coulombic efficiency (**Figure 2a**).[34, 42-44] After the formation cycles, there are negligible differences in the Coulombic efficiency (**Figure S2**), indicating that the decomposition predominates in the initial cycles.[42, 44]

Although decomposition is unavoidable, lithium residuals do not negatively impact capacity decay, resulting in similar capacity retentions of 73.7%, 70.1%, and 68.7% for the

samples aged in the Ar glovebox, in the dry box, and in the fresh state, respectively (**Figure 2b**). According to many studies, surface contaminants increase the ion diffusion energy barrier[36, 45] and promote increased amounts of gas generation (i.e. CO_2),[29, 42-44] which ultimately contributes to battery volume expansion. Degassing process after formation cycles is commonly adopted before the battery sealing, which adds to the battery cost.[46] Thus, washing cathode powders using water, alcohol, or other solvents,[29, 38] or a simple high temperature annealing under oxygen flow can be utilized to remove the lithium residues.[30, 31] We also noticed that upon extensive storage (three months in the dry box), the large amount of carbonates can be visible in the SEM (scanning electron microscopy) images, which would more negatively impact the battery performance (**Figure S3**).[31, 34, 37] Given that these materials are sensitive to storage environment and duration, it is recommended that scientific publications should specify these details when the performance is reported.

Sample preparation for surface structural and chemical characterization

　　　　Our previous studies suggest that Ti doping can enhance the surface stability of Ni-rich layered oxides, such as $LiNiO_2$ and NMC811, because of the improved surface oxygen retention.[14, 47] Here, we developed a direct approach to visualize the surface stability. Sonication is commonly utilized to break apart particle agglomerations to prepare scanning transmission electron microscopy (STEM) samples. Extensive sonication may trigger surface changes in $LiNiO_2$-based materials. Indeed, we observed a mossy surface after 30 minutes of sonication of Mg/Ti-$LiNiO_2$[14] in isopropyl alcohol (IPA) (**Figure 3a**), which likely resulted from lithium extraction and carbonate formation. It is consistent with the O K-edge soft XAS data showing an increased carbonate peak accompanied by the decreased hybridization peak (**Figure S4**). Meanwhile, the layered structure underwent surface reconstruction by which the surface-most region (2–5 nm depth) possessed a rock-salt structure (**Figures 3b-c**). The fast Fourier transform (FFT) patterns further confirmed that the surface reconstruction took place during the sonication while the bulk remained the layered structure (**Figure 3d-e**). In contrast, after $LiNiO_2$ was sonicated in IPA for 30 minutes (**Figure 3f-h**), the surface reconstruction layer was as deep as 20 nm, which was much thicker than the Mg/Ti-$LiNiO_2$. The STEM image indicates the presence of several atomic layers of spinel-like phase bridging the layered and rocksalt phases in the two materials.
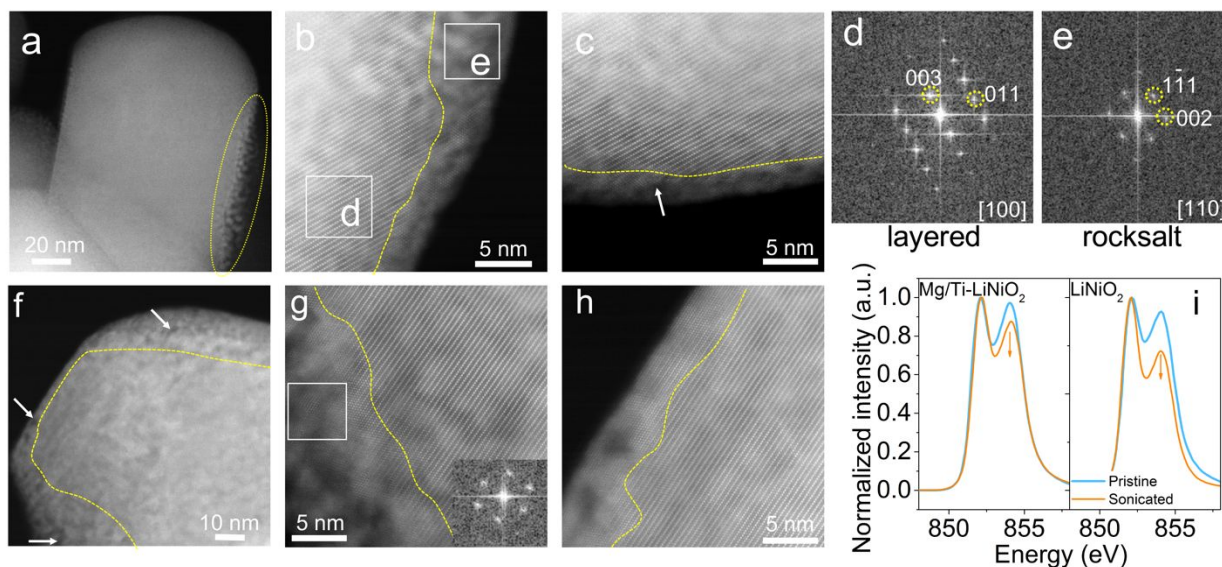
Figure 3 Characterizations of the Mg/Ti-LiNiO$_2$ and LiNiO$_2$ samples after sonication, (**a-c**) STEM images of the Mg/Ti-LiNiO$_2$ sonicated in IPA for 30 minutes, and the corresponding (**d-e**) FFT patterns from the selected areas (the zone axis of d is slightly off the [100]). Additionally, (**f-h**) STEM images of the LiNiO$_2$ sonicated in IPA for 30 minutes, the inserted FFT pattern is from the white square region in the figure g. (**i**) Soft XAS Ni L$_3$-edge spectra in the TEY mode of the samples before (pristine) and after sonication.

As illustrated by the dark contrast regions, many nanopores were generated within the surface-most 20 nm, indicated by the white arrows in **Figure 3f**. The pore formation is likely due to the depletion of lithium and oxygen. This corroborates previous reports that similar materials under high temperature or radiation, or at deep electrochemically delithiated conditions may promote pore formation.[48, 49] The formation mechanism is likely associated with lithium vacancy migration, oxygen release, and rock-salt formation.[48, 50, 51] Additionally, the decreased peak intensity in the Ni L$_3$-edge (~854 eV) illustrated surface nickel reduction and reconstruction (**Figure 3i**).[8] In general, the soft XAS Ni L$_3$ right/left peak ratio can qualitatively demonstrate the Ni oxidation state, with a higher value representing a higher oxidation state. Thus, less transition metal reduction was confirmed in the sonicated Mg/Ti-LiNiO$_2$ than that in the sonicated LiNiO$_2$ (**Figure S5**). By comparing the results, we present that the enhanced surface stability may be associated with Mg/Ti dual dopants, i.e., dual dopants can modify the electronic configuration which enhances the interfacial stability.[14, 47, 52, 53]

This simple, yet methodical sonication method can be applied to evaluate the surface stability of inorganic materials. In particular, the agglomerated secondary particles require a dispersing process to prepare samples for the TEM analysis. In addition, an extended sonication may be necessary in the cycled electrodes because of the binder usage. Our results have also shown that the surface of layered oxide materials can be easily influenced by the sonication method. Furthermore, our previous study also demonstrated that the cathode surface can be transformed by simply soaking layered oxide powders in organic solvents, including typical electrolyte solvents.[8, 40, 54, 55] With the inherent surface fragility of Ni-rich oxide materials, it is crucial to take cautions in preparing samples for characterization. Alternatively, many studies have applied focused ion beam (FIB) to prepare thin samples for TEM experiments. In this case, the chemical and structural information around grain boundaries can be protected for TEM analysis. However, it is not clear how the surface region may be influenced by the typical FIB coating protection and sample handling.

Doping Effect

Doping chemistry is one of the most popular methods to enhance the surface and bulk stability.[13, 14, 17, 47, 52, 53, 56, 57] Here we report how the surface characterization can reflect the different surface stability between doped and non-doped $LiNiO_2$. Both $LiNiO_2$ and Mg/Ti-$LiNiO_2$ have the typical layered structure with a $R\overline{3}m$ space group, as shown by X-ray diffraction (XRD) patterns (**Figure S6**).[14] Nevertheless, for the non-doped $LiNiO_2$ particles, a surface spinel-like layer is present, while the bulk structure remains layered (**Figures 4a, S7 a-d**). In contrast, the layered structure extends through the surface of the Mg/Ti-$LiNiO_2$ particles (**Figures 4b, S7 e-h**), suggesting the enhanced surface stability obtained through the Mg/Ti dual dopants. To obtain ensemble-averaged information, we used the soft XAS analysis to decouple surface and subsurface chemistries in these materials.[55] As shown in **Figure 4c**, the O K-edge pre-edge in the fluorescence yield (FY) mode consists of three features that are associated with the hybridization of $Ni^{3+}3d–O2p$ (~528 eV), $Ni^{2+}3d–O2p$ (~531 eV), and carbonate species (~534 eV).[58] The Mg/Ti dual dopants reduced the bulk cation mixing (Li^+/Ni^{2+}), as indicated by the decreased peak intensity at ~531 eV representing the hybridization of $Ni^{2+}3d$ and O2p. The increased extent of bulk cation mixing in $LiNiO_2$ was further confirmed by the slightly lower Ni oxidation state in $LiNiO_2$ than that in Mg/Ti-$LiNiO_2$ (**Figure 3i and Figure S5**). Furthermore, the Mg/Ti-$LiNiO_2$ material had a larger

(003)/(104) peak ratio in the XRD pattern, also suggesting globally inhibited cation mixing (**Figure S6**), which is consistent with the Rietveld refinement of neutron diffraction (ND) (**Figure S8**). Collectively, these results show that Mg/Ti dual dopants inhibit the cation mixing and promote the surface structural stability.
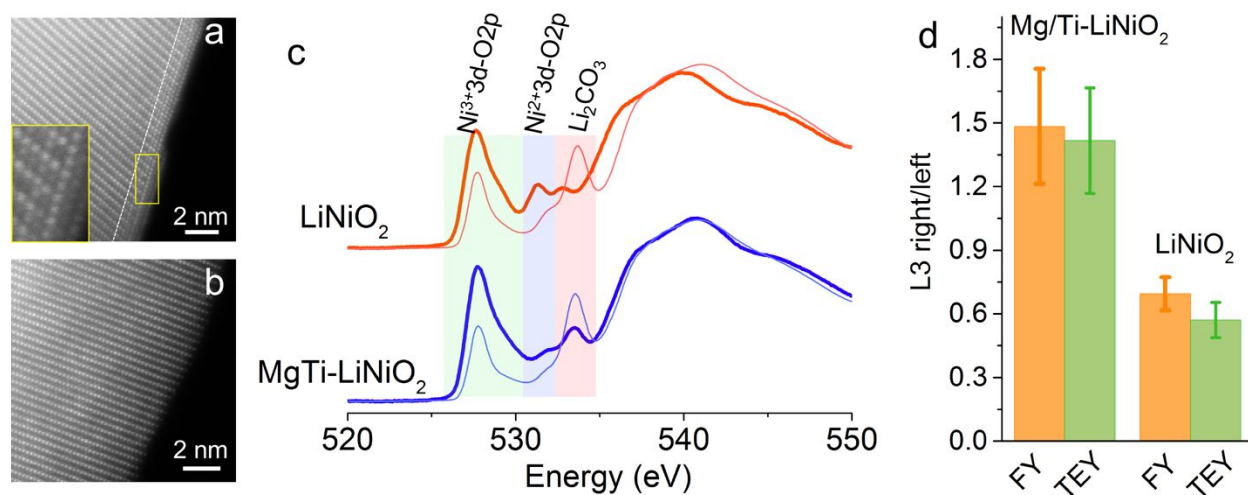
Figure 4 Comparative results of the Mg/Ti-LiNiO$_2$ and LiNiO$_2$ samples. Representative HAADF-STEM images of the **a**) LiNiO$_2$ and **b)** Mg/Ti-LiNiO$_2$ primary particles. **c**) Soft XAS O K-edge spectra in the FY (thick lines) and TEY (thin lines) modes. **d)** Ni L$_3$ right/left peak ratios from Ni soft XAS spectra of the charged Mg/Ti-LiNiO$_2$ and LiNiO$_2$ electrodes at 4.4 V vs Li/Li$^+$ in the second charge. Error bars are created based on the standard deviation of three repeated measurements.

The Mg/Ti dual dopants also enhance the surface stability even upon deep electrochemical delithiation. Here we found that *ex situ* soft XAS surface analysis may provide misleading results if the charged electrodes are not handled properly. In principle, Ni should experience oxidation during charging and reduction during discharging. However, due to the cathode–electrolyte parasitic reaction, the surface nickel oxidation state at various charge/discharge states were lower than that of the bulk (**Figure S9**). Another phenomenon that we constantly observe is that the Ni oxidation states for the charged samples were lower than that at the pristine state in both the TEY and FY modes (**Figure S9**), which is counterintuitive. We believe that this might be due to the thermodynamically unstable Ni^{4+} continually reacting with the electrolyte during the cell teardown and subsequent sample handling. Thus, eliminating the cell resting time and removing the residual

electrolyte are critical for maintaining the true Ni oxidation states for soft XAS analysis. We found that the best practice is to dissemble the cell and rinse the electrode immediately after the cell has reached the designated state of charge. This practice is particularly important for the charged electrodes. Here we rinsed the cycled electrode in an Ar filled glove box immediately after the cells were charged to 4.4 V vs Li/Li^+. The $LiNiO_2$ delivered a higher charge capacity at this upper cutoff voltage than the Mg/Ti-$LiNiO_2$ (**Figure S10**). If the surface was stable at the charged state, the Ni oxidation state at the surface should not exhibit significant difference in these two electrodes, because the charge capacity only differed by 22 mAh/g (i.e., the Ni oxidation state differed by 0.08). However, we found drastic differences between these electrodes, as explained below. The Ni L_3-right/left peak ratios were averaged from three electrodes at the charged state. A significantly higher L_3-right/left peak ratio in both FY and TEY modes was found in the Mg/Ti-$LiNiO_2$ sample than that in the $LiNiO_2$ sample (**Figure 4d**), indicating enhanced surface stability of the Mg/Ti-$LiNiO_2$ sample in the charged state. Moreover, the low L_3-right/left peak ratio in the FY mode of the $LiNiO_2$ electrodes also suggests that the surface reaction induced Ni reduction extended to the deep subsurface. The direct comparison between NMC622 and NMC811 (**Figure S11**) further supports that a higher nickel content results in more surface instability, which can potentially complicate the state of charge assessment using the surface sensitive soft XAS technique. As more studies have made use of the soft XAS technique for analyzing the surface chemistry of battery materials, our results clearly demonstrate that caution is needed when interpreting the data. Although the synchrotron characterization is not highly accessible, other surface-sensitive characterization methods, e.g., XPS, IR, Raman, TEM, ToF-SIMS, also encounter the similar challenges when preparing/handling samples. To improve the data representativeness, the effective error analysis, based on repeated measurements, is recommended.

Electrochemistry

In our previous work, it was confirmed that nickel redox (Ni^{3+}/Ni^{4+}) is the main contributor to the capacity of the $LiNiO_2$ based Co-free cathode materials.[13, 14] However, the parasitic reactions between the cathode and electrolyte lead to degraded surfaces with reduced nickel and reconstruction layer, impeding the battery stability. The surface instability of Co-free Ni-rich layered cathodes can become more severe at elevated temperatures through accelerating chemical/electrochemical reactions. Thus, we evaluated and compared the cycling performance of

the Mg/Ti-LiNiO$_2$ cathode at the temperatures of 22 and 60 °C. The elevated temperature facilitated the reversible capacity, indicated by the slightly higher discharge capacity of ~220 mAh g^{-1} at C/10 (**Figure 5a**) compared to the cell cycled at 22 °C with a discharge capacity of ~208 mAh g^{-1}.[14] However, the lower initial Coulombic efficiency of ~70% (~86% for the cells at 22 °C) suggests the combination of accelerated side reactions and electrolyte decomposition.[14, 59] The charge/discharge profiles in the initial 10 cycles overlapped well (**Figure 5a**). At the current rate of C/3, the capacity retention at 60 °C was much lower than that at 22 °C after 100 cycles (**Figure 5b**, the capacity retentions were 72% and 93% of the cells cycled at 60 °C and 22°C, respectively), which agrees with our previous study.[59] These results present the challenge that the LiNiO$_2$ based materials face at elevated temperatures.
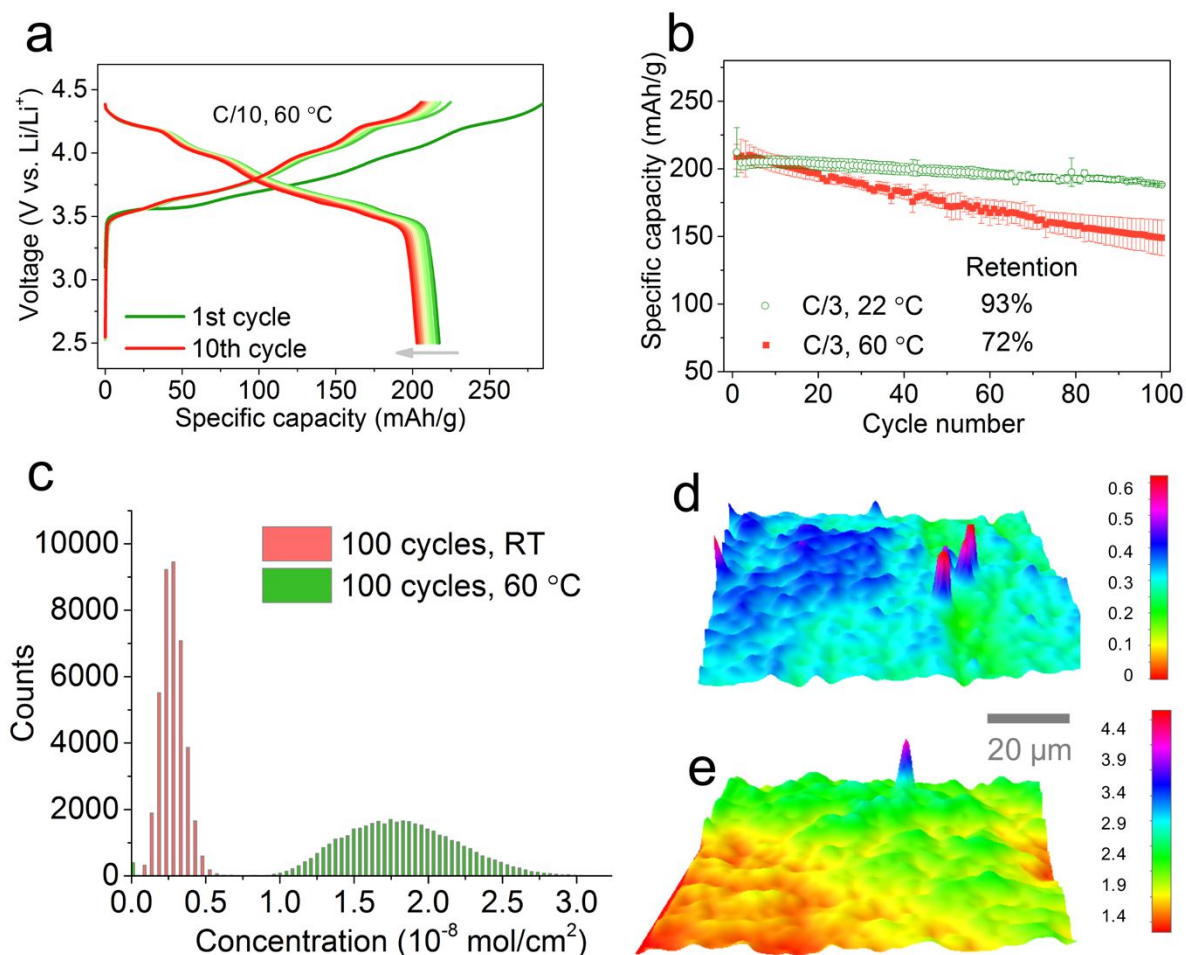
Figure 5 Surface degradation is accelerated at the elevated temperature. **a)** charge/discharge profiles of the cell containing Mg/Ti-LiNiO$_2$ cathode at C/10 at 60 °C, **b)** the comparison of the

cycling stability of the cells operated at 22 °C and 60 °C, where three individual cells were averaged and error bars are created based on the standard deviation, **c)** concentration histogram of the Ni deposited on the Li anodes cycled against the Mg/Ti-LiNiO$_2$ cathode at different temperatures, the Ni concentration (unit: 10^{-8} mol/cm^2) distribution on the Li anodes cycled at **d)** 22 °C and **e)** 60 °C.

Metal dissolution (nickel in this case), representing one aspect of surface instability, can be studied through performing X-ray fluorescence microscopy (XFM) measurements on the cycled anodes to quantitatively analyze the Ni dissolution at different temperatures.[13, 14] The Ni concentrations (**Figure 5c**) on the counter Li anodes distributed within 0–5 and 10–28 nmol/cm^2, giving an average concentration of 3.12 and 18.16 nmol/cm^2 at 22 °C and 60 °C, respectively. The concentration of nickel deposited on the lithium anode at 60 °C was roughly six times higher than that at 22 °C. Additionally, we found that the Ni distribution on the Li anodes was highly inhomogeneous for both cases (**Figure 5d-e**). The observation may be associated with the inhomogeneous solid electrolyte interface (SEI) formation. The cathode–electrolyte interface (CEI) can be easily disrupted at the elevated temperature, which exposes freshly reactive surfaces that subsequently undergoes continuously interfacial reactions, accelerating the degradation process.[59] The multiplied nickel concentration on the anode side is one consequence of the unstable CEI at 60 °C.

Conclusion

Co-free Ni-rich cathode materials, particularly LiNiO$_2$ and its doped analogs, face ongoing challenges as the need for commercialization rises. To address surface instability and its associated phenomena, a systematic and accurate understanding is highly required. In this work, we systematically studied the fragile surfaces of the LiNiO$_2$-based cathode materials, with the goal of identifying how experimental conditions may influence characterization results. We presented the challenges in characterizing and analyzing the surface chemistry of LiNiO$_2$-based materials using two comparative cathodes as a model platform, i.e., LiNiO$_2$ versus Mg/Ti-LiNiO$_2$. The surface lithium residuals are inevitable and highly dependent on various sample storage and handling conditions. Due to the highly reactive surfaces, we found that the sample preparation for electron

microscopy and surface-sensitive X-ray analyses greatly influences the final observations, resulting in skewed surface chemistry analytical results. We also provided some recommendations regarding how to obtain representative characterization analyses. Using simple comparisons, we further illustrated the advantages of Mg/Ti dual dopants to enhance the surface structural resistance to many circumstances, while corroborating previously reported observations.[13, 14, 53] However, we found that the surface of Mg/Ti-LiNiO$_2$ material still encounters a series of problems caused by the fragile CEIs at elevated temperatures. Efforts should be devoted towards the development of highly stable CEIs either by cathode surface coating, doping, electrolyte modification or combining multiple strategies.

Materials synthesis

The LiNiO$_2$ and Mg/Ti-LiNiO$_2$ were synthesized through a co-precipitation method followed by a high-temperature calcination, which can be found in our previous studies.[13, 14]

Characterizations

X-ray photoelectron spectroscopy (XPS): XPS characterization was performed on a PHI Versa Probe III scanning XPS microscope using monochromatic Al K-alpha X-ray source (1486.6 eV). Samples were transferred from an Ar-filled glove box to the XPS ultrahigh vacuum chamber via a vacuum transfer vessel. The probing depths of C1s, Li1s, and O1s XPS are similar. X-ray absorption spectroscopy (XAS): Soft XAS measurements were performed on the 31-pole wiggler beamline 10^{-1} at Stanford synchrotron radiation light source (SSRL). All spectra were normalized by the current from freshly evaporated gold on a fine grid positioned upstream of the main chamber. XAS samples were mounted on an aluminum sample holder with double-sided carbon tape in a Ar-filled glove box and transferred to the load-lock chamber in a double-contained container, using a glove bag purged with nitrogen for the transfer. X-ray fluorescence microscopy (XFM): The X-ray fluorescence mapping was measured at the microprobe hard X-ray 2-ID-D beamline at the Advanced Photon Source. The samples are raster-scanned by a sub-micrometer focused X-ray beam with 10 keV photon energy. The fluorescent X-rays are detected by a single element Si-drift Vortex detector. All images presented in this work covers a 100 μm × 100 μm area with 0.5 μm × 0.5 μm pixel size. Scanning transmission electron microscopy (STEM): STEM was acquired on a JEOL 2100 S/TEM operated at 200 keV. Scanning electron microscopy (SEM):

The morphologies of the materials were investigated using a scanning electron microscope (SEM) (LEO FESEM) at an accelerating voltage of 5 kV. Neutron diffraction (ND): ND was conducted using the ECHIDNA high-resolution powder diffractometer (Australian Nuclear Science and Technology Organization). A wavelength of 1.6215Å was used for the measurement and each pattern was recorded for 3.5 h. The data set was further refined using GSAS EXPGUI. X-ray diffraction (XRD): The XRD patterns were collected at the beam line 11-3 at Stanford Synchrotron Radiation Lightsource (SSRL) with an X-ray wavelength of 0.976 Å.

Electrochemical characterization

The cathode materials were processed into the electrodes immediately following high temperature calcination or after the designated handling history. The acetylene carbon and poly(vinylidene difluoride) (PVdF) were stored in a humidity controlled dry box prior to the electrode preparation. The composite cathodes were prepared by spreading the slurry (N-methyl-2-pyrrolidone as the solvent) with active material (90 wt %), acetylene carbon (5 wt %), and PVdF binder (5 wt %), and casted on carbon-coated aluminum foils. The cathode electrodes were punched into disks of a diameter of 10 mm. The disks were then dried overnight at 120 °C in a vacuum oven and transferred into a Ar-filled glove box. The cathode active mass loading was ~6 mg/cm^2. CR2032 coin cells were assembled in a Ar filled glovebox using the composite cathode, the lithium foil anode, Whatman glass fiber (1827-047934-AH) as the separator, and 1 M LiPF$_6$ dissolved in ethylene carbonate (EC) and ethyl methyl carbonate (EMC) with 2 wt % vinylene carbonate (VC) as the electrolyte (the weight ratio of EC:EMC is 3:7). All cells were cycled with an electrochemical workstation (Wuhan Land Company) at 22 °C and 60 °C in an environmental chamber. The specific energy was calculated using the LANDdt software. 1C was defined as fully charging a cathode in 1 h, corresponding to a specific current density of 200 mA/g.

Acknowledgements

This report was prepared as an account of work sponsored by an agency of the United States Government. Neither the United States Government nor any agency thereof, nor any of their employees, makes any warranty, express or implied, or assumes any legal liability or responsibility for the accuracy, completeness, or usefulness of any information, apparatus, product, or process disclosed, or represents that its use would not infringe privately owned rights. Reference herein to any specific commercial product, process, or service by trade name, trademark, manufacturer, or otherwise does not necessarily constitute or imply its endorsement, recommendation, or favoring by the United States Government or any agency thereof. The views and opinions of authors expressed herein do not necessarily state or reflect those of the United States Government or any agency thereof.

Author contributions

F.L. conceived and led the project. L.M. and F.L. designed the experiments. L.M. performed the synthesis, SEM, synchrotron, and electrochemical measurements. L.T. and Z.X. performed the human exhalation experiments and XPS analysis. L.L. performed XFM experiments. Z.Y., Y.D. and H.L.X. conducted the STEM experiments. S.S. and D.N. performed the soft XAS measurements. L.M., C.K.W. and F.L. wrote the manuscript with the help of all the authors.

Declaration of Interests

The authors declare no competing interests.

References

1.　M. Bianchini, M. Roca-Ayats, P. Hartmann, T. Brezesinski and J. Janek, There and Back Again-The Journey of $LiNiO_2$ as a Cathode Active Material, *Angew Chem Int Ed Engl*, 2019, **58**, 10434-10458.

2.　H. Li, N. Zhang, J. Li and J. R. Dahn, Updating the Structure and Electrochemistry of $LixNiO_2$ for $0 \leqslant x \leqslant 1$, *J. Electrochem. Soc.*, 2018, **165**, A2985-A2993.

3.　C. S. Yoon, D.-W. Jun, S.-T. Myung and Y.-K. Sun, Structural Stability of $LiNiO_2$ Cycled above 4.2 V, *ACS Energy Lett.*, 2017, **2**, 1150-1155.

4.　M. Li and J. Lu, Cobalt in lithium-ion batteries, *Science*, 2020, **367**, 979.

5.　J. Zheng, W. H. Kan and A. Manthiram, Role of Mn Content on the Electrochemical Properties of Nickel-Rich Layered $LiNi_{0.8-x}Co_{0.1}Mn_{0.1+x}O_2$ $(0.0 \leqslant x \leqslant 0.08)$ Cathodes for Lithium-Ion Batteries, *ACS Appl. Mater. Interfaces*, 2015, **7**, 6926-6934.

6.　L. Liang, W. Zhang, F. Zhao, D. K. Denis, F. u. Zaman, L. Hou and C. Yuan, Surface/Interface Structure Degradation of Ni-Rich Layered Oxide Cathodes toward Lithium-Ion Batteries: Fundamental Mechanisms and Remedying Strategies, *Adv. Mater. Interfaces*, 2019, **7**, 1901749.

7.　K. Kim, H. Ma, S. Park and N.-S. Choi, Electrolyte Additive-Driven Interfacial Engineering for High-Capacity Electrodes in Lithium-Ion Batteries: Promise and Challenges, *ACS Energy Lett.*, 2020, **5**, 1537-1553.

8.　F. Lin, I. M. Markus, D. Nordlund, T.-C. Weng, M. D. Asta, H. L. Xin and M. M. Doeff, Surface reconstruction and chemical evolution of stoichiometric layered cathode materials for lithium-ion batteries, *Nat. Commun.*, 2014, **5**, 3529.

9.　P. Yan, J. Zheng, M. Gu, J. Xiao, J. G. Zhang and C. M. Wang, Intragranular cracking as a critical barrier for high-voltage usage of layer-structured cathode for lithium-ion batteries, *Nat. Commun.*, 2017, **8**, 14101.

10.　J. M. Lim, T. Hwang, D. Kim, M. S. Park, K. Cho and M. Cho, Intrinsic Origins of Crack Generation in Ni-rich $LiNi_{0.8}Co_{0.1}Mn_{0.1}O_2$ Layered Oxide Cathode Material, *Sci. Rep.*, 2017, **7**, 39669.

11.　C. Tian, Y. Xu, D. Nordlund, F. Lin, J. Liu, Z. Sun, Y. Liu and M. Doeff, Charge Heterogeneity and Surface Chemistry in Polycrystalline Cathode Materials, *Joule*, 2018, **2**, 464-477.

12.　H. Li, M. Cormier, N. Zhang, J. Inglis, J. Li and J. R. Dahn, Is Cobalt Needed in Ni-Rich Positive Electrode Materials for Lithium Ion Batteries?, *J. Electrochem. Soc.*, 2019, **166**, A429-A439.

13.　L. Mu, W. H. Kan, C. Kuai, Z. Yang, L. Li, C.-J. Sun, S. Sainio, M. Avdeev, D. Nordlund and F. Lin, Structural and Electrochemical Impacts of Mg/Mn Dual Dopants on the $LiNiO_2$ Cathode in Li-Metal Batteries, *ACS Appl. Mater. Interfaces*, 2020, **12**, 12874-12882.

14.　L. Mu, R. Zhang, W. H. Kan, Y. Zhang, L. Li, C. Kuai, B. Zydlewski, M. M. Rahman, C.-J. Sun, S. Sainio, M. Avdeev, D. Nordlund, H. L. Xin and F. Lin, Dopant Distribution in Co-Free High-Energy Layered Cathode Materials, *Chem. Mater.*, 2019, **31**, 9769-9776.

15.　H.-H. Ryu, G.-T. Park, C. S. Yoon and Y.-K. Sun, Suppressing detrimental phase transitions via tungsten doping of $LiNiO_2$ cathode for next-generation lithium-ion batteries, *J. Mater. Chem. A*, 2019, **7**, 18580-18588.

16.　Y. Kim, Effects and distribution of Zr introduced in Ni-based cathode material for Li-ion batteries, *Phy. Chem. Chem. Phy.*, 2019, **21**, 12505-12517.

17.   M. M. E. Cormier, N. Zhang, A. Liu, H. Li, J. Inglis and J. R. Dahn, Impact of Dopants (Al, Mg, Mn, Co) on the Reactivity of Li_xNiO_2 with the Electrolyte of Li-Ion Batteries, *J. Electrochem. Soc.*, 2019, **166**, A2826-A2833.

18.   T. Deng, X. Fan, L. Cao, J. Chen, S. Hou, X. Ji, L. Chen, S. Li, X. Zhou, E. Hu, D. Su, X.-Q. Yang and C. Wang, Designing In-Situ-Formed Interphases Enables Highly Reversible Cobalt-Free $LiNiO_2$ Cathode for Li-ion and Li-metal Batteries, *Joule*, 2019, **3**, 2550-2564.

19.   W. Zhao, J. Zheng, L. Zou, H. Jia, B. Liu, H. Wang, M. H. Engelhard, C. Wang, W. Xu, Y. Yang and J.-G. Zhang, High Voltage Operation of Ni-Rich NMC Cathodes Enabled by Stable Electrode/Electrolyte Interphases, *Adv. Energy Mater.*, 2018, **8**, 1800297.

20.   E. Markevich, G. Salitra, Y. Talyosef, U.-H. Kim, H.-H. Ryu, Y.-K. Sun and D. Aurbach, High-Performance $LiNiO_2$ Cathodes with Practical Loading Cycled with Li metal Anodes in Fluoroethylene Carbonate-Based Electrolyte Solution, *ACS Appl. Energy Mater.*, 2018, **1**, 2600-2607.

21.   B. Xiao and X. Sun, Surface and Subsurface Reactions of Lithium Transition Metal Oxide Cathode Materials: An Overview of the Fundamental Origins and Remedying Approaches, *Adv. Energy Mater.*, 2018, **8**.

22.   F. Kong, C. Liang, L. Wang, Y. Zheng, S. Perananthan, R. C. Longo, J. P. Ferraris, M. Kim and K. Cho, Kinetic Stability of Bulk $LiNiO_2$ and Surface Degradation by Oxygen Evolution in $LiNiO_2$-Based Cathode Materials, *Adv. Energy Mater.*, 2019, **9**, 1802586.

23.   L. Zheng, L. Li, R. Shunmugasundaram and M. N. Obrovac, Effect of Controlled-Atmosphere Storage and Ethanol Rinsing on $NaNi_{0.5}Mn_{0.5}O_2$ for Sodium-Ion Batteries, *ACS Appl. Mater. Interfaces*, 2018, **10**, 38246-38254.

24.   J. Eom, M. G. Kim and J. Cho, Storage Characteristics of $LiN_{0.8}Co_{0.1+x}Mn_{0.1-x}O_2$ (x=0, 0.03, and 0.06) Cathode Materials for Lithium Batteries, *J. Electrochem. Soc.*, 2008, **155**.

25.   R. Jung, R. Morasch, P. Karayaylali, K. Phillips, F. Maglia, C. Stinner, Y. Shao-Horn and H. A. Gasteiger, Effect of Ambient Storage on the Degradation of Ni-Rich Positive Electrode Materials (NMC811) for Li-Ion Batteries, *J. Electrochem. Soc.*, 2018, **165**, A132-A141.

26.   S. W. Song, G. V. Zhuang and P. N. Ross, Surface Film Formation on $LiNi_{0.8}Co_{0.15}Al_{0.05}O_2$ Cathodes Using Attenuated Total Reflection IR Spectroscopy, *J. Electrochem. Soc.*, 2004, **151**.

27.   B. Huang, K. Qian, Y. Liu, D. Liu, K. Zhou, F. Kang and B. Li, Investigations on the Surface Degradation of $LiNi_{1/3}Co_{1/3}Mn_{1/3}O_2$ after Storage, *ACS Sustain. Chem. Eng.*, 2019, **7**, 7378-7385.

28.   H. Ren, Y. Huang, Y. Wang, Z. Li, P. Cai, Z. Peng and Y. Zhou, Effects of different carbonate precipitators on $LiNi_{1/3}Co_{1/3}Mn_{1/3}O_2$ morphology and electrochemical performance, *Mater. Chem. Phys.*, 2009, **117**, 41-45.

29.   S. E. Renfrew, L. A. Kaufman and B. D. McCloskey, Altering Surface Contaminants and Defects Influences the First-Cycle Outgassing and Irreversible Transformations of $LiNi_{0.6}Mn_{0.2}Co_{0.2}O_2$, *ACS Appl. Mater. Interfaces*, 2019, **11**, 34913-34921.

30.   B. Huang, D. Liu, K. Qian, L. Zhang, K. Zhou, Y. Liu, F. Kang and B. Li, A Simple Method for the Complete Performance Recovery of Degraded Ni-rich $LiNi_{0.70}Co_{0.15}Mn_{0.15}O_2$ Cathode via Surface Reconstruction, *ACS Appl. Mater. Interfaces*, 2019, **11**, 14076-14084.

31.　　H. Liu, Y. Yang and J. Zhang, Investigation and improvement on the storage property of $LiNi_{0.8}Co_{0.2}O_2$ as a cathode material for lithium-ion batteries, *J. Power Sources*, 2006, **162**, 644-650.

32.　　H.-J. Noh, S. Youn, C. S. Yoon and Y.-K. Sun, Comparison of the structural and electrochemical properties of layered $Li[Ni_xCo_yMn_z]O_2$ (x=1/3, 0.5, 0.6, 0.7, 0.8 and 0.85) cathode material for lithium-ion batteries, *J. Power Sources*, 2013, **233**, 121-130.

33.　　L. Baggetto, N. J. Dudney and G. M. Veith, Surface chemistry of metal oxide coated lithium manganese nickel oxide thin film cathodes studied by XPS, *Electrochim. Acta*, 2013, **90**, 135-147.

34.　　C. Wang, L. Shao, X. Guo, X. Xi, L. Yang, C. Huang, C. Zhou, H. Zhao, D. Yin and Z. Wang, Air-Induced Degradation and Electrochemical Regeneration for the Performance of Layered Ni-Rich Cathodes, *ACS Appl. Mater. Interfaces*, 2019, **11**, 44036-44045.

35.　　H. Liu, Y. Yang and J. Zhang, Reaction mechanism and kinetics of lithium ion battery cathode material $LiNiO_2$ with CO_2, *J. Power Sources*, 2007, **173**, 556-561.

36.　　A. Grenier, H. Liu, K. M. Wiaderek, Z. W. Lebens-Higgins, O. J. Borkiewicz, L. F. J. Piper, P. J. Chupas and K. W. Chapman, Reaction Heterogeneity in $LiNi_{0.8}Co_{0.15}Al_{0.05}O_2$ Induced by Surface Layer, *Chem. Mater.*, 2017, **29**, 7345-7352.

37.　　H. S. Liu, Z. R. Zhang, Z. L. Gong and Y. Yang, Origin of Deterioration for $LiNiO_2$ Cathode Material during Storage in Air, *Electrochem. Solid-State Lett.*, 2004, **7**.

38.　　X. Zheng, X. Li, Z. Wang, H. Guo, Z. Huang, G. Yan and D. Wang, Investigation and improvement on the electrochemical performance and storage characteristics of $LiNiO_2$-based materials for lithium ion battery, *Electrochim. Acta*, 2016, **191**, 832-840.

39.　　L. Zou, Y. He, Z. Liu, H. Jia, J. Zhu, J. Zheng, G. Wang, X. Li, J. Xiao, J. Liu, J.G. Zhang, G. Chen, C. Wang, Nat. Commun., 2020, 11, 3204.

40.　　P. Oh, B. Song, W. Li and A. Manthiram, Overcoming the chemical instability on exposure to air of Ni-rich layered oxide cathodes by coating with spinel $LiMn_{1.9}Al_{0.1}O_4$, *J. Mater. Chem. A*, 2016, **4**, 5839-5841.

41.　　S. E. Renfrew and B. D. McCloskey, Residual Lithium Carbonate Predominantly Accounts for First Cycle CO_2 and CO Outgassing of Li-Stoichiometric and Li-Rich Layered Transition-Metal Oxides, *J. Am. Chem. Soc.*, 2017, **139**, 17853-17860.

42.　　L. de Biasi, A. Schiele, M. Roca-Ayats, G. Garcia, T. Brezesinski, P. Hartmann and J. Janek, Phase Transformation Behavior and Stability of $LiNiO_2$ Cathode Material for Li-Ion Batteries Obtained from In Situ Gas Analysis and Operando X-Ray Diffraction, *ChemSusChem*, 2019, **12**, 2240-2250.

43.　　S. E. Renfrew and B. D. McCloskey, Quantification of Surface Oxygen Depletion and Solid Carbonate Evolution on the First Cycle of $LiNi_{0.6}Mn_{0.2}Co_{0.2}O_2$ Electrodes, *ACS Appl. Energy Mater.*, 2019, **2**, 3762-3772.

44.　　K. Qian, B. Huang, Y. Liu, M. Wagemaker, M. Liu, H. Duan, D. Liu, Y.-B. He, B. Li and F. Kang, Increase and discretization of the energy barrier for individual $LiNi_xCo_yMn_yO_2$ (x+2y=1) particles with the growth of a Li_2CO_3 surface film, *J. Mater. Chem. A*, 2019, **7**, 12723-12731.

45.　　J.-Y. Cherng, C.-T. Hu, W.-C. Chiang and N.-Y. Liu, Degassing method for lithium battery cell, *European patent*, 2017, EP3416230A3416231.

46.　　J. D. Steiner, H. Cheng, J. Walsh, Y. Zhang, B. Zydlewski, L. Mu, Z. Xu, M. M. Rahman, H. Sun, F. M. Michel, C.-J. Sun, D. Nordlund, W. Luo, J.-C. Zheng, H. L. Xin and F. Lin, Targeted Surface Doping with Reversible Local Environment Improves Oxygen Stability

at the Electrochemical Interfaces of Nickel-Rich Cathode Materials, *ACS Appl. Mater. Interfaces*, 2019, **11**, 37885-37891.

47. L. Mu, R. Lin, R. Xu, L. Han, S. Xia, D. Sokaras, J. D. Steiner, T.-C. Weng, D. Nordlund, M. M. Doeff, Y. Liu, K. Zhao, H. L. Xin and F. Lin, Oxygen Release Induced Chemomechanical Breakdown of Layered Cathode Materials, *Nano Lett.*, 2018, **18**, 3241-3249.

48. M. M. Rahman, W.-Y. Chen, L. Mu, Z. Xu, Z. Xiao, M. Li, X.-M. Bai and F. Lin, Defect and structural evolution under high energy ion irradiation informs battery materials design for extreme environments, *submitted*, 2020.

49. E. Hu, X. Yu, R. Lin, X. Bi, J. Lu, S. Bak, K.-W. Nam, H. L. Xin, C. Jaye, D. A. Fischer, K. Amine and X.-Q. Yang, Evolution of redox couples in Li- and Mn-rich cathode materials and mitigation of voltage fade by reducing oxygen release, *Nat. Energy*, 2018, **3**, 690-698.

50. P. Yan, J. Zheng, Z. K. Tang, A. Devaraj, G. Chen, K. Amine, J. G. Zhang, L. M. Liu and C. Wang, Injection of oxygen vacancies in the bulk lattice of layered cathodes, *Nat Nanotechnol*, 2019, **14**, 602-608.

51. L. Zou, J. Li, Z. Liu, G. Wang, A. Manthiram and C. Wang, Lattice doping regulated interfacial reactions in cathode for enhanced cycling stability, *Nat. Commun.*, 2019, **10**, 3447.

52. J.-N. Zhang, Q. Li, C. Ouyang, X. Yu, M. Ge, X. Huang, E. Hu, C. Ma, S. Li, R. Xiao, W. Yang, Y. Chu, Y. Liu, H. Yu, X.-Q. Yang, X. Huang, L. Chen and H. Li, Trace doping of multiple elements enables stable battery cycling of $LiCoO_2$ at 4.6 V, *Nat. Energy*, 2019, **4**, 594-603.

53. L. Mu, M. M. Rahman, Y. Zhang, X. Feng, X. Du, D. Nordlund and F. Lin, Surface transformation by a "cocktail" solvent enables stable cathode materials for sodium ion batteries, *J. Mater. Chem. A*, 2018, **6**, 2578-2766.

54. F. Lin, D. Nordlund, I. M. Markus, T.-C. Weng, H. L. Xin and M. M. Doeff, Profiling the nanoscale gradient in stoichiometric layered cathode particles for lithium-ion batteries, *Energy Environ. Sci.*, 2014, **7**, 3077-3085.

55. L. Mu, X. Feng, R. Kou, Y. Zhang, H. Guo, C. Tian, C.-J. Sun, X.-W. Du, D. Nordlund, H. L. Xin and F. Lin, Deciphering the Cathode–Electrolyte Interfacial Chemistry in Sodium Layered Cathode Materials, *Adv. Energy Mater.*, 2018, **8**, 1801975.

56. Q. Liu, X. Su, D. Lei, Y. Qin, J. Wen, F. Guo, Y. A. Wu, Y. Rong, R. Kou, X. Xiao, F. Aguesse, J. Bareño, Y. Ren, W. Lu and Y. Li, Approaching the capacity limit of lithium cobalt oxide in lithium ion batteries via lanthanum and aluminium doping, *Nat. Energy*, 2018, **3**, 936-943.

57. Q. Xie, W. Li and A. Manthiram, A Mg-Doped High-Nickel Layered Oxide Cathode Enabling Safer, High-Energy-Density Li-Ion Batteries, *Chem. Mater.*, 2019, **31**, 938-946.

58. C. Tian, D. Nordlund, H. L. Xin, Y. Xu, Y. Liu, D. Sokaras, F. Lin and M. M. Doeff, Depth-Dependent Redox Behavior of $LiNi_{0.6}Mn_{0.2}Co_{0.2}O_2$, *J. Electrochem. Soc.*, 2018, **165**, A696-A704.

59. J. D. Steiner, L. Mu, J. Walsh, M. M. Rahman, B. Zydlewski, F. M. Michel, H. L. Xin, D. Nordlund and F. Lin, Accelerated Evolution of Surface Chemistry Determined by Temperature and Cycling History in Nickel-Rich Layered Cathode Materials, *ACS Appl. Mater. Interfaces*, 2018, **10**, 23842-23850.